IOP Publishing Measurement Science and Technology
Meas. Sci. Technol. **32** (2021) 115119 (11pp) https://doi.org/10.1088/1361-6501/ac0bde

Broadband elastic wave detection based on dual FBGs capable of automatically matching the spectra

Fu Tongling[1,2], Chen Ting[1], Li Jian[1] and Huang Xinjing[1,*]

[1] State Key Laboratory of Precision Measuring Technology and Instruments, Tianjin University, Tianjin 300072, People's Republic of China
[2] Tianjin Key Laboratory of Microgravity and Hypogravity Environment Simulation Technology, Tianjin 300072, People's Republic of China

E-mail: huangxinjing@tju.edu.cn

Received 21 March 2021, revised 5 June 2021
Accepted for publication 16 June 2021
Published 4 August 2021

Abstract

Fiber Bragg grating (FBG)-based sensors can be used to detect middle/high frequency elastic waves via intensity demodulation. Temperature change or structural deformation at the location where the sensing FBG is adhered to may shift the FBG spectrum and mismatch the interrogator filter and sensing FBG spectra, leading to sensing failure. This paper proposes a broadband elastic wave measurement system with a trackable work point based on dual FBGs together with a piezoelectric transducer (PZT), wherein one FBG is pasted on the PZT as a filter and tracker. By applying AC + DC excitation to the PZT and sweeping the DC bias, the two FBGs' spectra are autonomously matched by searching the max amplitude of the receiving AC signals to maintain high sensitivity. It is experimentally demonstrated that the proposed system can detect up to 500 kHz broadband elastic waves. The proposed system is replicated to produce four sets that are successfully used to detect and locate the impact on an aluminum plate.

Keywords: FBG, optic fiber, PZT, elastic wave

(Some figures may appear in colour only in the online journal)

1. Introduction

The use of elastic waves plays an important role in structural health monitoring, such as structural deformation detection, leak detection, impact detection, and defect detection. A traditional elastic wave sensor is a piezoelectric transducer (PZT). The PZT has a structural resonance frequency, which can only work around several discrete frequencies and is susceptible to electromagnetic interference [1–3]. Unlike the PZT, fiber Bragg grating (FBG) is soft, and FBG-based sensors have a flat frequency response to elastic waves or dynamic strains with different frequencies. Moreover, FBG has strong anti-electromagnetic interference ability, is lightweight and corrosion resistant, and has been widely used in the field of structural health monitoring of pressure vessels, pipelines, bridges, railroad tracks, etc [4–6].

One of the key challenges when using FBG-based sensors is demodulation of the wavelength-encoded signal to effectively extract the elastic wave information. Since elastic waves are broadband, from a few kHz to several MHz, absolute wavelength demodulation (AWD) methods are incompetent due to low demodulation speed [7–10]. AWD needs to sweep the light-source wavelength with the help of a tunable laser, a tunable Fabry–Perot filter, or even a spectrometer to determine the center wavelength change in the sensing FBG, and the wavelength sweeping speed is very slow. FBG-based elastic wave detection usually employs edge filtering methods, which are also called intensity demodulation methods [11–13]. The edge filtering methods use a narrowband tunable laser or a broadband light source with an optical filter to tune the narrowband peak to the left or right slope in the main lobe of the FBG spectrum.

* Author to whom any correspondence should be addressed.

Temperature change or structural deformation at the location where the sensing FBG is adhered may shift the FBG spectrum and lead to a mismatch between the interrogator filter spectrum and the FBG spectrum. To avoid such a mismatch, one alternative solution is to adhere the ordinary light-transmitting optical fiber to the surface of the object to be monitored to receive and transmit elastic waves to the sensing FBG, ensuring that the sensing FBG does not contact the object [14–17].The modal composition in the sensing fiber may be influenced by the material properties and geometry of the fiber and its coating [16]. Another alternative solution is to use dual FBGs: one for sensing, and the other for compensation [18–21]. Dual FBGs can effectively compensate for the center wavelength shift caused by environmental temperature changes, but cannot compensate for the center wavelength changes caused by structural deformation or FBG adhering stress. To match the interrogator filter spectrum with that of the sensor FBG, the compensation FBG can be stretched or compressed using a linear PZT stack driven by a DC power supply [13] to shift its center wavelength. How to autonomously adjust the wavelength spectrum and achieve the wavelength match within the process of field use is still an unresolved problem.

This paper proposes an elastic wave measurement system based on dual FBGs + PZT, in which one FBG is pasted on the PZT as a filter and tracker. By applying AC excitation to the PZT and sweeping the DC bias, the center wavelength of the reference FBG is adjusted and the spectra of the two FBGs are automatically matched, to realize the tracking of the operating point of the system and maintain high sensitivity. This method has the advantages of a trackable operating point, low cost, broadband, and temperature compensation. This paper will introduce the working principle of the method, test its performance in detection of broadband elastic waves, and demonstrate its application in impact sound source localization.

2. Working principle

A schematic of the proposed FBG-based elastic wave detection system is shown in figure 1. Light from a broadband superluminescent diode (Thorlabs, S5FC1005S) is sent to a filter FBG via a fiber circulator. Its center wavelength is 1550 nm and the bandwidth is 50 nm, which meets the multiplexing requirements of multiple FBGs. The narrowband reflected light from the filter FBG is then coupled to a sensing FBG via another fiber circulator. The reflected light from the sensing FBG sensor is the overlapping part of the two FBG spectra. The overlapping light enters a photodetector (PD) (New Focus, 2053-FC) and is converted into an electrical signal, which is collected by a data acquisition card (DAQ card, National Instruments, USB-6366) that is connected to a personal computer. The elastic wave can induce a slight shift to the wavelength spectrum of the sensing FBG, which results in the intensity fluctuation of the final reflected light that is detected by the PD. The filter FBG is adhered to a 7 × 7 × 20 mm stacked PZT (PST150, 28 μm/200 V). The filter FBG is used to monitor and track the work point of the dual FBG sensing

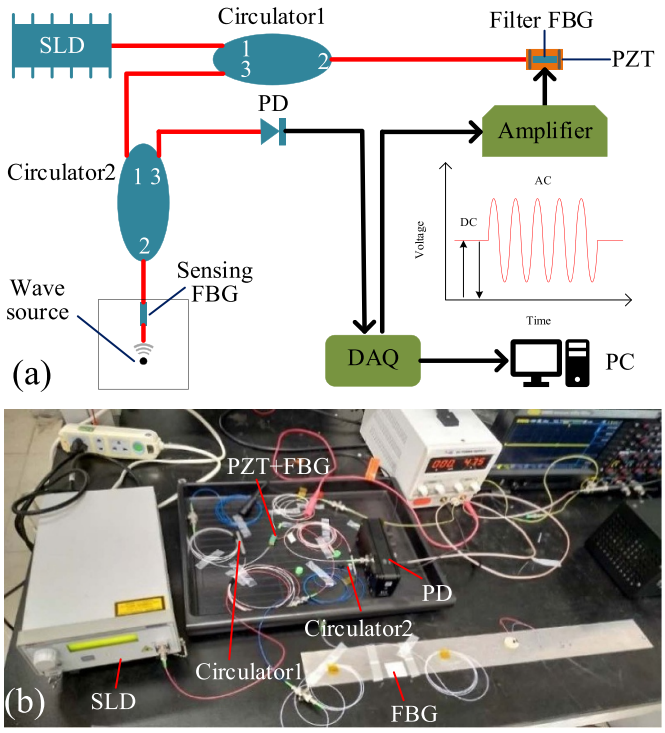

Figure 1. The demodulation system diagram (a) and apparatus (b).

system by adjusting the drive voltage to keep the two FBGs' spectra at their quadrature points. The FBG is a uniform type. Its length is 10 mm. Its wavelength is 1550 nm. Its 3 dB bandwidth is 0.2 nm. Its reflectivity is more than 90%. Its side-mode suppression ratio is 20 dB.

As shown in figure 2, when the central wavelength difference between the two FBGs is reasonably set, the output of the PD can accurately reflect the dynamic strain and has high sensitivity. When the selected wavelength difference is not appropriate, not only will the sensitivity of the system be greatly reduced, sensing signal distortion will also occur. To obtain high sensitivity, the central wavelength of one FBG should be set near the 3 dB position of the other FBG's spectrum, rather than having the two spectra exactly coincide with each other. There is no accurate expression of the spectrum of the FBG once pasted for calculation of the working point. This paper proposes an experimental method to search and track the best matching position of the two spectra in quasi-real time. Experimental results show that the wavelength difference between the two FBGs should be about 0.3 nm.

Specifically, the DAQ card generates an AC + DC signal which is amplified by the voltage amplifier and then sent to the PZT actuator to track the work point. The small AC voltage component can cause the PZT to vibrate, thus generating an 'ostensible' elastic wave whose frequency is already known onto the filter FBG that is detected by the PD. Keeping the AC amplitude constant, the DC voltage component is swept until the maximum amplitude of the PD output at that frequency is found. Then, the DC component is kept unchanged and the AC component is closed. In this case, if an elastic wave stretches/compresses the sensing FBG, the PD will output a noticeable AC signal. In this case, maximum sensitivity is

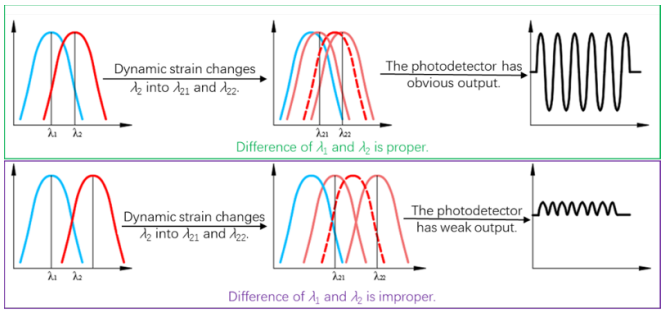

Figure 2. The influence of spectral difference in the FBG-pair on measured waves.

Table 1. Searching the best driving voltage[a].

U_d	U_{PD}	U_d	U_{PD}	U_d	U_{PD}	U_d	U_{PD}
0	0.818	8	1.493	16	1.920	24	1.564
1	0.889	9	1.564	**17**	**1.955**	25	1.493
2	0.960	10	1.635	18	1.884	26	1.422
3	1.066	11	1.706	19	1.849	27	1.351
4	1.137	12	1.778	20	1.813	28	1.244
5	1.244	13	1.849	21	1.742	29	1.173
6	1.315	14	1.884	22	1.706	30	1.066
7	1.386	15	1.884	23	1.671	31	0.960

[a] : U_d—driving voltage; U_{PD}—Output amplitude of the PD; unit: V.
Note: U_{PD} reaches its max value of 1.955 when U_d is 17 V.

achieved, indicating the success of the work point tracking procedure. Table 1 shows an example of searching the best driving voltage. The AC component is 1 Vpp and the DC component is swept from 0 V to 35 V. The PD output reaches its maximum amplitude when the DC offset is 17 V. Then, the best work point is successfully tracked by keeping the DC offset of 17 V unchanged and removing the AC component output.

An experiment demonstrating the advantage of working point traceability was carried out. The experimental setup is shown in figures 3(a) and (b). A metal block and a limiting part are used to bend the aluminum plate with different deflections. When the aluminum plate is not bent and the spectra of the two FBGs match each other, the measured elastic wave signal is large, as shown in figure 3(c). When the aluminum plate is bent, the center wavelength of the sensing FBG moves, the spectra of the two FBGs no longer match, and the measured signal becomes weaker and even disappears, as shown in figures 3(d) and (e). Then, the steps described above are used to search and adjust the operating point of the system so that the spectra of the two FBGs match each other. Finally, the amplitude of the detected elastic wave signal is restored to the original magnitude, as shown in figure 3(f).

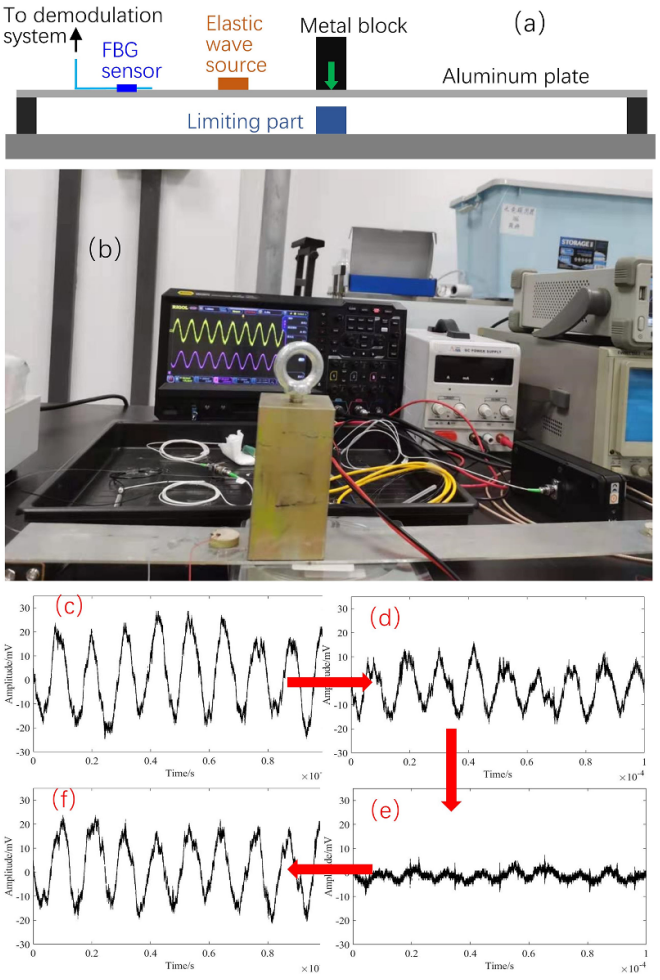

Figure 3. The experiment demonstrating the advantage of working point traceability.

3. Performance tests

3.1. Broadband elastic wave detection

Different specifications of PZTs were used to stimulate elastic waves of different frequencies on an aluminum plate to test the ability of the dual FBG system to detect broadband elastic waves. The distance between the PZT and the sensing FBG is 100 mm, the aluminum plate size is 500 × 50 × 2 mm, and the FBG's grating area is 10 mm long. A total of nine different frequencies of elastic waves were tested: 7 kHz, 58 kHz, 100 kHz, 200 kHz, 300 kHz, 350 kHz, 400 kHz, 450 kHz, and 500 kHz. These frequencies are the resonant frequencies of several PZTs. The driving voltages sent to the PZT to stimulate different elastic waves of each frequency have identical amplitudes. The elastic wave reflected from the boundary of the aluminum plate will form enhanced interference and destructive interference in the aluminum plate. The energy distribution of the elastic wave in the aluminum plate is not uniform and will change with the change in the excitation frequency. Therefore, for each test frequency, the PZT needs to be moved to find a measurement point with a relatively large elastic wave amplitude. The collected signals in the time domain and their corresponding frequency spectra are shown in figure 4. It can be seen that elastic waves of each frequency can be clearly detected, but the amplitude is different and the waveform is distorted. It is preliminarily speculated that the amplitude difference in the received signal at different frequencies is due to the different abilities of each PZT to stimulate elastic waves. The test results demonstrate the system's ability to detect broadband

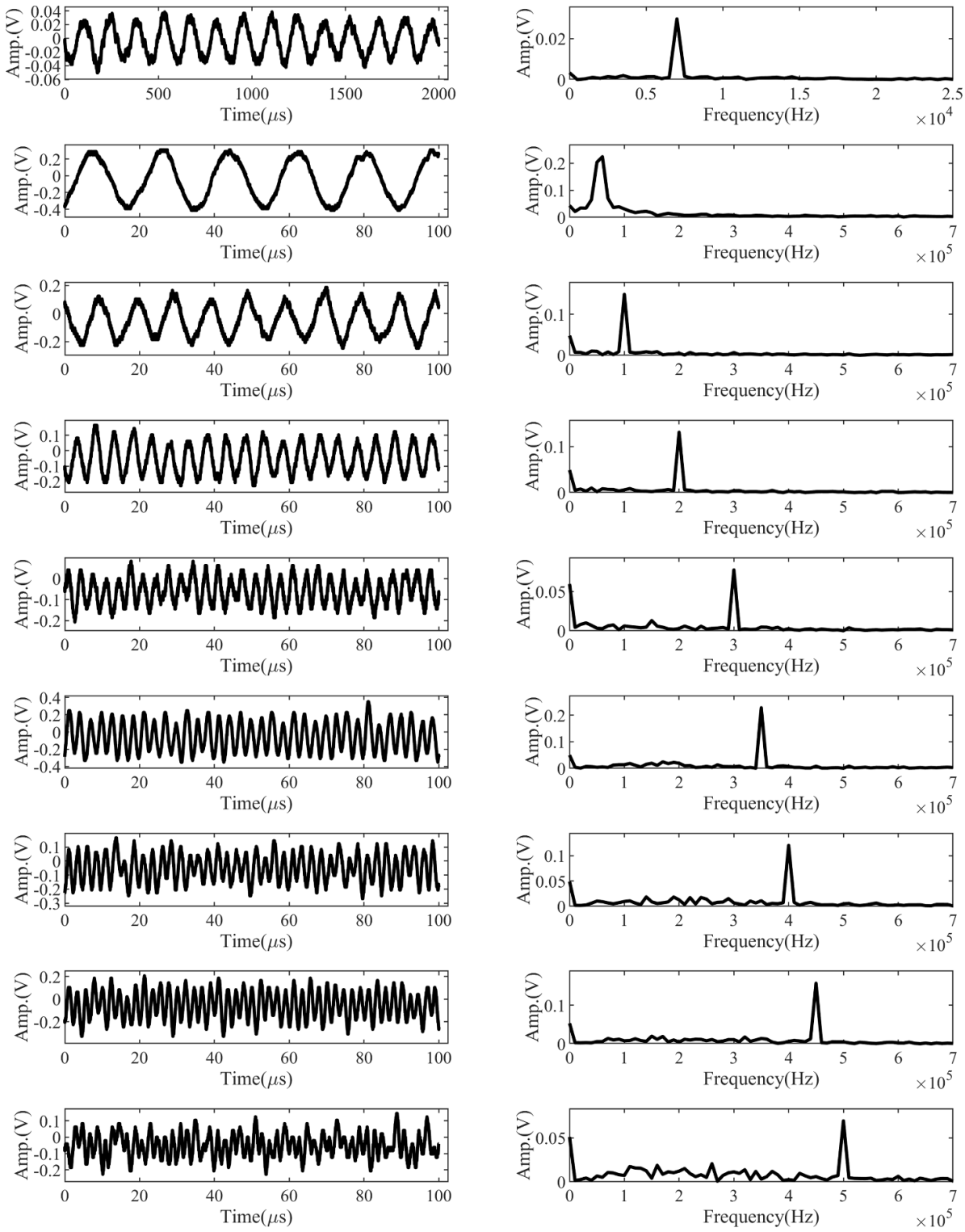

Figure 4. Elastic wave signals measured at different frequencies.

elastic waves, but whether its frequency response is flat or not still requires further confirmation.

3.2. Comparison with a laser Doppler vibrometer (LDV)

To further verify whether the frequency response of the system to elastic waves is flat and its ability to perceive pulse elastic waves, a comparison experiment using FBG and an LDV to simultaneously measure elastic waves was carried out; the experiment apparatus is shown in figure 5. The experiment still used the 500 × 50 × 2 mm aluminum plate. To make the measurement conditions of the sensing FBG and the LDV as similar as possible, the sensing FBG and the laser spot were symmetrically arranged on two sides of the PZT (the elastic

Figure 5. A schematic of the comparison experiment between FBG and the LDV.

wave source), as shown in figure 5. UV glue was used to paste the sensing FBG onto the aluminum plate, Couplant was used between the aluminum plate and the PZT to generate more noticeable elastic waves in the aluminum plate. A signal generator was used to output eight cycles of sine signals with a frequency of 7 kHz–500 kHz and an amplitude of 1 Vpp. After being amplified by a power amplifier, the signal was sent to the PZT to generate elastic waves in the aluminum plate. The purpose of using pulse trains instead of continuous sinusoidal signals is to reduce the influence of reflections in the plate on the measurement results, so that the measurement results of the two methods are more comparable. Signals of several frequencies are shown in figure 6. It can be seen that two groups of signals collected by the FBG sensor and LDV with the frequencies of 10 kHz, 58 kHz, 100 kHz, 300 kHz, and 500 kHz have similar waveforms.

The frequency spectra of the time domain signals obtained by the two methods are calculated as follows: denoting the frequency of each excitation signal as f_0, the amplitude of the frequency spectrum in the range of $[0.9f_0, 1.1f_0]$ is intercepted and the average value is calculated. The results are shown in table 2. The output voltage of the LDV is proportional to the vertical displacement of the aluminum plate surface, and the output voltage of the FBG system's PD is approximately proportional to the in-plane strain of the surface. In theory, there is a proportional relationship between the vertical displacement and the in-plane strain at the two symmetric measurement points, so the ratio of the output voltage of the two measurement systems should be approximately flat. The amplitude ratio of the two methods at different frequencies is listed in table 2. It can be observed that the ratio is higher at 58 kHz and 70 kHz, and lower at 7 kHz and 10 kHz, but the overall ratio fluctuation is approximately in the range of 3.82–43.43. Although the ratio is not so flat, the FBG system can still capture clear elastic waves at different frequencies. Frequency detection errors are listed in table 3. The max error is 3%. These frequency errors originate from the amplitude fluctuations caused by multiple echo mixing, and the frequency of the detection signal is slightly moved by amplitude modulation. The ability of the system to measure broadband elastic waves is demonstrated.

4. Application in impact localization

Spacecraft in orbit may be hit and damaged by flying space debris, so it is necessary to monitor and locate the impact. The impact will cause broadband elastic waves that propagate on the aluminum alloy shell. The detection and positioning of impact can be realized by using elastic wave signals at multiple measuring points with known positions. Impact positioning experiment apparatus was designed and built as shown in figure 7. The test aluminum plate is 500 × 500 × 2 mm, and its center is defined as the origin of the coordinate system. A total of four dual-FBG elastic wave measurement systems were built. A light source was input to the four-way system through a four-channel optical splitter. The four sensing FBGs are respectively arranged at A (0, 200), B (−200, 0), C (0, −200), and D (200, 0), and the unit is mm. The filters of four PDs were set to be 1–300 kHz, and the magnifications were set to be 3×10^3. The four filter FBGs are attached to the four PZTs, respectively. A steel ball with a diameter of 6 mm fell freely from a height of 15 cm and hit the aluminum plate. To ensure the repeatability of multiple impact tests, a test tube clamp is used to fix a cylindrical tube as a trajectory for the falling ball. In this experiment, propagation attenuation of the elastic waves in such a small aluminum plate is very small. Therefore, the impact-induced elastic waves are always detectable and their amplitude fluctuations have little influence on the positioning accuracy. The impact location test involves two steps: (a) measuring the group velocity of the impact-induced elastic waves; (b) using the hyperbolic intersection method [22] to calculate the location of the impact point.

First, elastic wave velocity measurement experiments were carried out. The aluminum plate is hit by the steel ball at

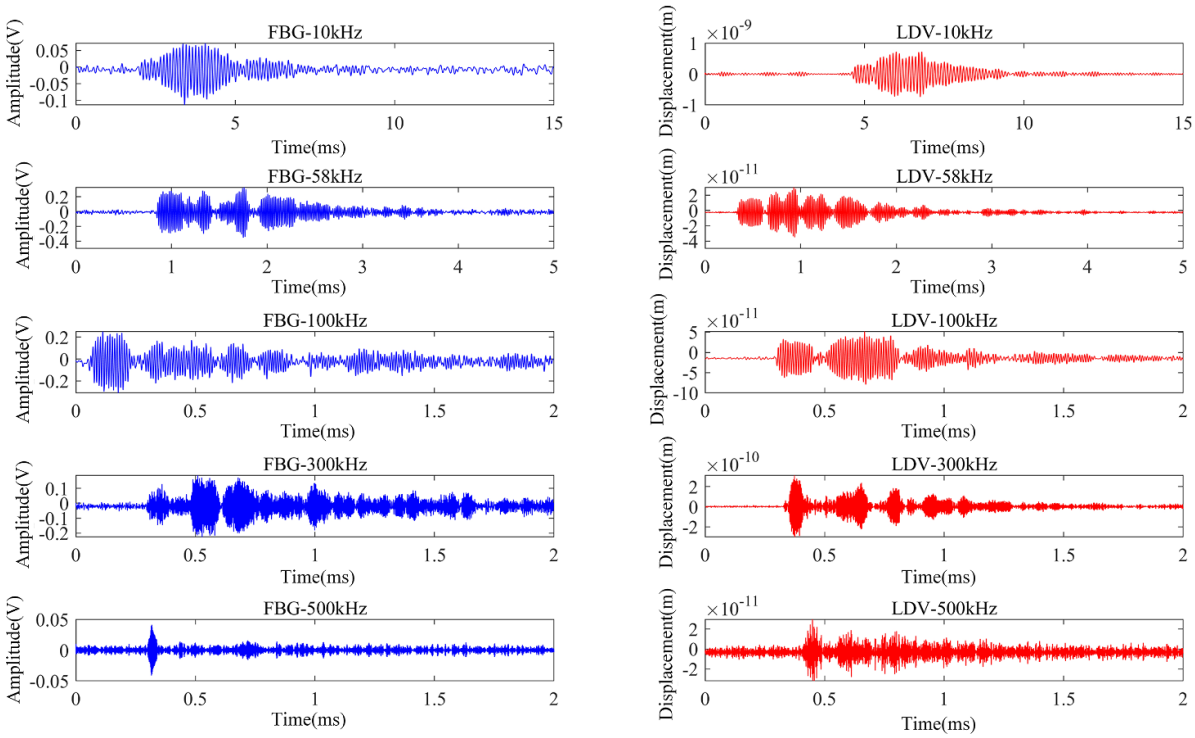

Figure 6. Signals with different frequencies measured by FBG (left) and the LDV (right).

Table 2. FBG and LDV comparison experiment results, Amp.

Freq. (kHz)	By FBG① (V)	By LDV② (m)	①/② (V m^{-1})	①/②/3.27E + 8
7	9.71E-04	2.97E-12	3.27E + 08	1.00
10	1.14E-03	9.30E-12	1.22E + 08	0.37
15	4.86E-03	3.89E-12	1.25E + 09	3.82
58	7.50E-03	6.25E-13	1.20E + 10	36.70
70	3.92E-03	2.75E-13	1.42E + 10	43.43
100	7.68E-03	1.75E-12	4.38E + 09	13.39
200	2.47E-03	2.41E-12	1.02E + 09	3.12
300	3.02E-03	2.93E-12	1.03E + 09	3.15
500	2.46E-04	1.67E-13	1.48E + 09	4.53

Table 3. FBG and LDV comparison experiment results, Freq.

Freq.③ (kHz)	By FBG④ (kHz)	By LDV⑤ (kHz)	(③−④)/③	(③−⑤)/③
7	7.1	7.1	−1.4%	−1.4%
10	9.9	9.9	1.0%	1.0%
15	15.0	14.9	0%	0.7%
58	57.8	58.0	0.3%	0.0%
70	71.0	68.0	−1.4%	2.9%
100	97.0	100.0	3.0%	0.0%
200	204.5	200.5	−2.3%	−0.3%
300	302.0	299.5	−0.7%	0.2%
500	495.0	490.5	1.0%	1.9%

E (0, 50), F (−50, 0), G (0, −50), and H (50, 0); the unit is mm. A DAQ card was used to collect four channels of signals simultaneously; the sampling rate is 1 MSps, and a segment of signals is shown in figure 8. The frequency spectra of the background noise and the impact signal are shown in figures 8(e) and (f). It can be seen that the impact signal is broadband up to 50 kHz. The Akaike information criterion algorithm [23] was used to calculate the start point of each impact signal, as shown by the red curves in figure 8. Time differences and elastic wave velocities of the four cases were calculated using the measured elastic waves. The velocity calculation expression and results are listed in table 4. The

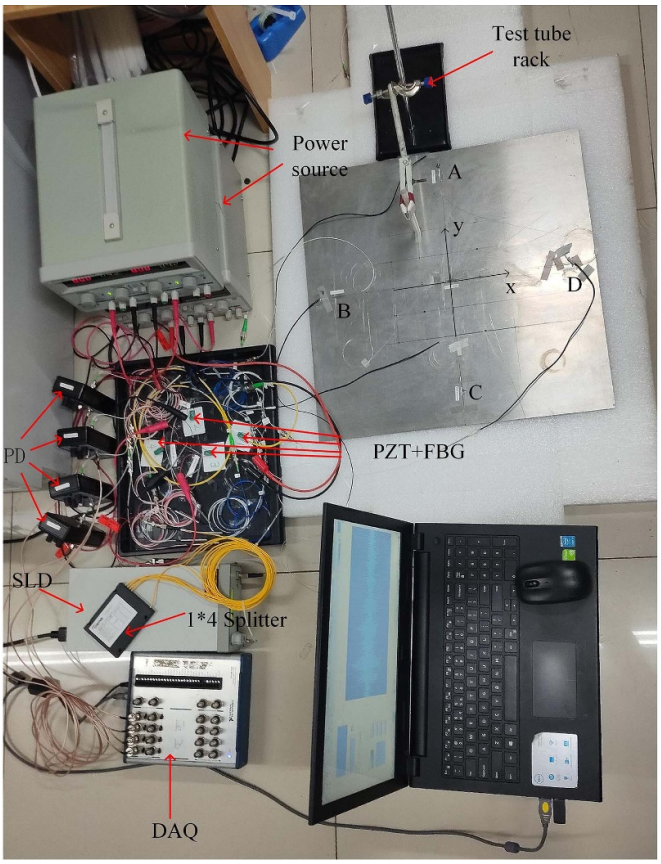

Figure 7. Experimental apparatus of the impact-localization tests.

average sound velocity of the impact-induced elastic wave is 1669 m s^{-1}. To further confirm the accuracy of the velocity measurement value, a group velocity dispersion curve of a 2 mm thick aluminum plate was calculated, and the results are shown in figure 9. There are two modes, S0 and A0, when the frequency is below 50 kHz. Since the unilateral impact is an asymmetric load, the excited elastic wave is mainly the asymmetric A0 mode, rather than the symmetric S0 mode. As the frequency increases, the group velocity of the A0 mode elastic wave increases. Therefore, the initial part of the signal corresponds to the fastest 50 kHz elastic wave. It can be seen from the dispersion curve that theoretically its group velocity is 1689 m s^{-1}, which is very close to the experimentally measured value. Therefore, in the impact positioning experiment, the propagation velocity of the impact-induced elastic wave uses the experimentally measured value of 1669 m s^{-1}.

Then, another four points were selected for impact-localization tests. Their coordinates were (50, 50), (−50, −50), (50, −100), and (−50, 100). The impact test at each point was repeated five times. The impact signals were recorded and were used to calculate the transit time difference, impact point position, and positioning error, as shown in table 5. The localization results are also plotted in a 2D plane, as shown in figure 10. It can be seen from table 5 that most of the points have high positioning accuracy, except for a few individual points.

In table 5, the average means that the five t_{AC} and t_{BD} are first averaged to obtain time differences with higher accuracy, and then the impact point position and positioning error are calculated using the new t_{AC} and t_{BD}. The positioning error is calculated as the difference between the coordinates of the actual impact point and the coordinates measured by the system. When the average value of the five time differences is used for positioning calculation, the positioning error is reduced to less than 5 mm. Considering the source of localization error, the first factor is that the impact signal was generated by manually placing a small ball in a tube to freely fall, which is prone to uncontrollable small lateral deviations; the second factor is that the propagation velocity of the elastic wave in the plate was considered as constant in the positioning calculation, but this velocity referred to broadband elastic waves and was not constant.

5. Further discussion of the upper frequency limit

This paper uses an intensity demodulation system, and its demodulation speed depends on the photoelectric conversion speed and the filter bandwidth of the circuit part. The PD model we use is a Newport 2053, and its comprehensive bandwidth is 10 MHz, which is high enough. In fact, FBG realizes the measurement of vibration or elastic waves by measuring dynamic strain. When the demodulation speed is fast enough, the highest frequency of dynamic strain that FBG can measure depends on the coupling method of dynamic strain and the ratio of the FBG length to the

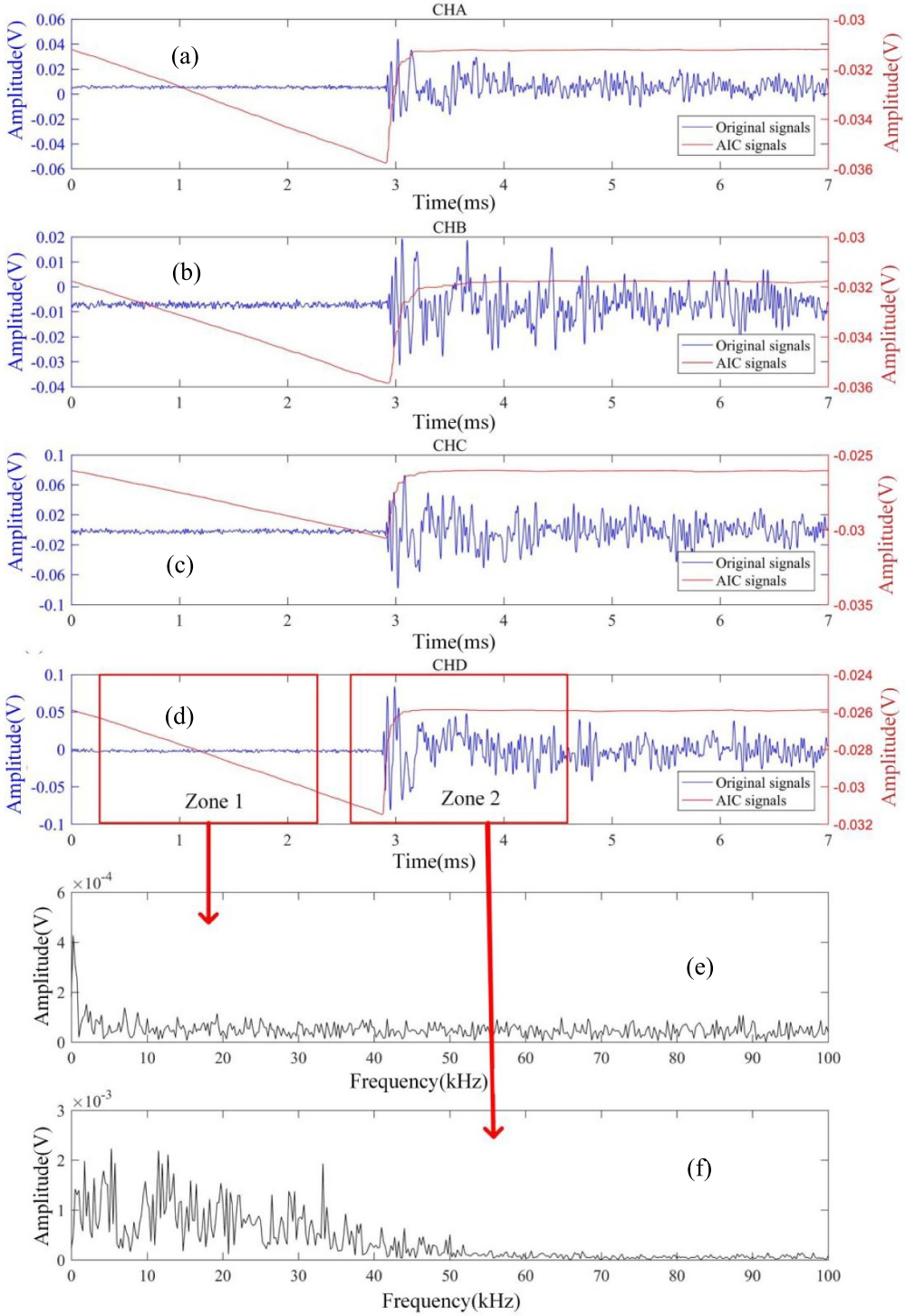

Figure 8. Impact-positioning test signals. (a) Signals in the time domain of CH_A. (b) Signals in the time domain of CH_B. (c) Signals in the time domain of CH_C. (d) Signals in the time domain of CH_D. (e) The spectrum of zone 1. (f) The spectrum of zone 2.

Table 4. Velocity measurement results of elastic waves caused by impacts.

No.	c_1 (m s^{-1})	c_2 (m s^{-1})	c_3 (m s^{-1})	c_4 (m s^{-1})
Expressions	$\frac{\lvert EC\rvert-\lvert EA\rvert}{\Delta t_{CA}}$	$\frac{\lvert GA\rvert-\lvert GC\rvert}{\Delta t_{AC}}$	$\frac{\lvert FD\rvert-\lvert FB\rvert}{\Delta t_{DB}}$	$\frac{\lvert HB\rvert-\lvert HD\rvert}{\Delta t_{BD}}$
Values (m s^{-1})	1655	1678	1704	1639
Average (m s^{-1})	1669			

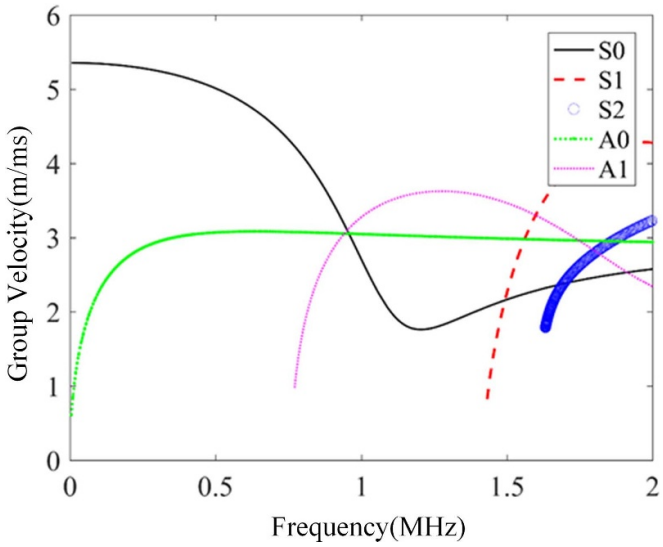

Figure 9. Dispersion curves of the 2 mm thick aluminum plate.

Table 5. Localization results of impact points.

Actual coordinates (mm)	Repetition no.	t_{AC} (ms)	t_{BD} (ms)	Measured coordinates (mm)	X error (mm)	Y error (mm)	Distance error (mm)
(50.00, 50.00)	1	0.05	−0.055	(42.91, 46.99)	7.09	3.01	7.7
	2	0.051	−0.064	(44.20, 54.76)	5.8	4.76	7.5
	3	0.054	−0.06	(46.61, 51.48)	3.39	1.48	3.7
	4	0.049	−0.062	(42.36, 52.94)	7.64	2.94	8.19
	5	0.063	−0.06	(54.45, 52.03)	4.45	2.03	4.89
Average		0.053	−0.060	(46.10, 51.62)	3.9	1.62	4.23
(−50.00, −50.00)	1	−0.063	0.057	(−54.27, −49.41)	4.27	0.59	4.31
	2	−0.063	0.05	(−53.88, −43.32)	3.88	6.68	7.73
	3	−0.064	0.053	(−54.91, −45.99)	4.91	4.01	6.34
	4	−0.061	0.049	(−52.11, −42.35)	2.11	7.65	7.94
	5	−0.063	0.064	(−54.71, −55.51)	4.71	5.51	7.25
Average		−0.063	0.055	(−53.96, −47.31)	3.96	2.69	4.79
(50.00, −100.00)	1	0.059	0.12	(55.90, −104.22)	5.9	4.22	7.25
	2	0.047	0.12	(44.27, −102.66)	5.73	2.66	6.32
	3	0.053	0.109	(49.08, −93.80)	0.92	6.2	6.27
	4	0.043	0.125	(40.81, −106.53)	9.19	6.53	11.28
	5	0.045	0.117	(42.13, −99.86)	7.87	0.14	7.88
Average		0.049	0.118	(46.43, −101.38)	3.57	1.38	3.83
(−50.00, 100.00)	1	−0.057	−0.113	(−53.25, 97.78)	3.25	2.22	3.94
	2	−0.054	−0.117	(−50.75100.89)	0.75	0.89	1.16
	3	−0.052	−0.105	(−47.80, 90.21)	2.2	9.79	10.03
	4	−0.059	−0.113	(−55.17, 98.04)	5.17	1.96	5.53
	5	−0.055	−0.112	(−51.24, 96.65)	1.24	3.35	3.58
Average		−0.055	−0.112	(−51.63, 96.7)	1.63	3.3	3.68

wavelength of the elastic wave. The ratio is preferably less than one. The elastic wave wavelength is related to the wave speed, and the wave speed has a complicated relationship with the size and material properties of the elastic wave waveguide and the guided wave modes, so it is difficult to quantitatively calculate the detectable upper frequency limit.

When the dynamic strain is excited laterally by external sound waves, as shown in [20], the FBG is compressed or stretched as a whole, and every point on the FBG is in phase. In this case, the sensitivity of the FBG sensor is independent of the dynamic strain wavelength, and the FBG can measure dynamic strain at very high frequencies. When the dynamic strain is propagated sequentially along the optical fiber, each point of the FBG is compressed or stretched sequentially. If the frequency is very low and the wavelength of the dynamic strain is very long, the phase difference between FBG points is very small and the FBG sensitivity is high. If the frequency is very

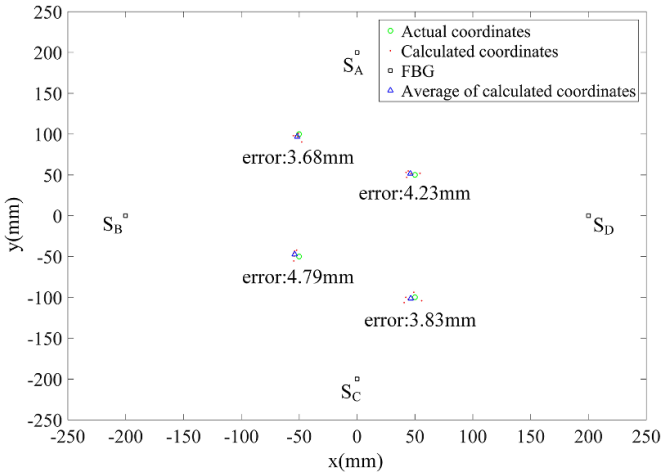

Figure 10. Localization results of impact points in a 2D plane.

high and the wavelength of the dynamic strain is very short, especially if it is shorter than the FBG, the phase difference between each point of the FBG is very large, and each point of the FBG is not compressed or stretched synchronously, the FBG sensitivity will be very low, and even no signal can be detected. The test conditions in this paper belong to the latter scenario. Therefore, [20] can measure the dynamic strain caused by underwater acoustic waves up to 5 MHz, while this paper can measure the dynamic strain caused by elastic waves up to 500 kHz. Reference [20] uses a structure to convert the excitation of underwater sound pressure into compression and elongation of the sensing FBG. The method in this paper directly pastes the sensing FBG onto the solid surface to sense elastic waves. Therefore, another advantage of the proposed method is simplicity of installation without any conversion structure required, in addition to the advantage that its working point is trackable.

6. Conclusion and future work

This paper has demonstrated a broadband elastic wave measurement system with a trackable work point based on dual FBGs + PZT. A pre-biased AC voltage signal is applied to the PZT where the sensing FBG is adhered. The peak-to-peak value of the AC component in the receiving signal indicates the sensitivity of the system with the current configuration. Adjusting the bias voltage to maximize the peak-to-peak value of the AC component can realize the tracking of the high sensitivity operating point when the spectra of the two FBGs are automatically matched. It is experimentally demonstrated that the proposed system can detect 7–500 kHz broadband elastic waves, including continuous elastic waves, pulse elastic waves, and impact elastic waves. The proposed system is replicated to produce four sets that are successfully used to detect and locate the impact on an aluminum plate. The system proves the feasibility of applications in structural health monitoring of in-orbit spacecraft. For the next step, the whole system will be miniaturized using an optoelectronic device and circuit customizations.

Data availability statement

All data that support the findings of this study are included within the article (and any supplementary files).

Acknowledgments

This work is supported by the National Key Research and Development Program of China (No. 2018YFC0808600), the National Natural Science Foundation of China (Nos. 61803280, 61973227), and the Open Project Program of Tianjin Key Laboratory of Microgravity and Hypogravity Environment Simulation Technology (No. TJWDZL2019KT006).

ORCID iD

Huang Xinjing https://orcid.org/0000-0002-8964-8502

References

[1] Krautkramer J and Krautkramer H 1969 *Ultrasonic Testing of Materials* (Berlin: SpringerVerlag)
[2] Zhao X, Gao H, Zhang G, Ayhan B, Yan F, Kwan C and Rose J L 2007 Active health monitoring of an aircraft wing with embedded piezoelectric sensor/actuator network: i. defect detection, localization and growth monitoring *Smart Mater. Struct.* **16** 1208–17
[3] Giurgiutiu V, Zagrai A and Bao J 2002 Piezoelectric wafer embedded active sensors for aging aircraft structural health monitoring *Struct. Health Monit.* **1** 41–61
[4] Betz D C, Thursby G, Culshaw B and Staszewski W J 2003 Acoustoultrasonic sensing using fiber Bragg gratings *Smart Mater. Struct.* **12** 122–8
[5] Wu Q, Okabe Y and Yu F 2018 Ultrasonic structural health monitoring using fiber Bragg grating *Sensors* **18** 3395
[6] Druet T, Chapuis B, Jules M, Laffont G and Moulin E 2018 Passive guided waves measurements using fiber Bragg gratings sensors *J. Acoust. Soc. Am.* **144** 1198–202
[7] Muller M S, Hoffmann L, Bodendorfer T, Hirth F, Petit F, Plattner M P, Buck T C and Koch A W 2010 Fiber-optic sensor interrogation based on a widely tunable monolithic laser diode *IEEE Trans. Instrum. Meas.* **59** 696–703
[8] Mohamed Nizar S and Elizabeth Caroline B 2019 Comparison of fiber optic sensors based on FBG—a review *2019 IEEE Int. Conf. on System, Computation, Automation and Networking (ICSCAN), Proc.* p 6
[9] Kong X 2019 *The High-speed Fiber Grating Demodulation Technology and Experimental Research Based on FPGA* (Shandong: Shandong University)
[10] Qin J, Yin J, Zhu Z and Tan D Y 2019 Development and application of new FBG mini tension link transducers for monitoring dynamic response of a flexible barrier under impact loads *Measurement* **153** 107409
[11] Lan L, Dong D, Chunliu Z, Yiling S, Shangzhong J and Zaixuan Z 2010 Research and development of intensity-modulated fiber Bragg grating sensors *Laser Optoelectron. Prog.* **47** 090603
[12] Dongsheng L, Sui Q M and Cao Y Q 2008 Linearity optimization of edge filter demodulators in FBGs *Optoelectron. Lett.* **4** 193–5
[13] Harish A V, Varghese B, Rao B, Balasubramaniam K and Srinivasan B 2015 Dynamic interrogator for elastic wave

sensing using Fabry Perot filters based on fiber Bragg gratings *Ultrasonics* **60** 103–8
[14] Lee J R, Lee S S and Yoon D J 2008 Simultaneous multipoint acoustic emission sensing using fibre acoustic wave grating sensors with identical spectrum *J. Opt.* A **10** 085307
[15] Wee J *et al* 2016 Increasing signal amplitude in fiber Bragg grating detection of Lamb waves using remote bonding *Appl. Opt.* **55** 5564–9
[16] Davis C, Rosalie C, Norman P, Rajic N, Habel J and Bernier M 2018 Remote sensing of lamb waves using optical fibres—an investigation of modal composition *J. Lightwave Technol.* **36** 2820–6
[17] Wee J, Alexander K and Peters K 2020 Self-referencing ultrasound detection of fiber Bragg grating sensor remotely bonded at two locations *Proc. SPIE* **11379** 113791F
[18] Shin C S and Chen B L 2011 An improved impact source locating system using FBG rosette array *Proc. SPIE* **8409** 84091B
[19] Gao X, Wang Y, Yuan B, Yuan Y, Dai Y and Xu G 2013 Low-cost vibration sensor based on dual fiber Bragg gratings and light intensity measurement *Appl. Opt.* **52** 6782–7
[20] Bai X *et al* 2018 A submerged optical fiber ultrasonic sensor using matched fiber Bragg gratings *Sensors* **18** 1942
[21] Xia D, Wei P and Chenggui L 2019 Difference between FBG and PZT acoustic emission sensor *Advances in Acoustic Emission Technology. Proc. World Conf. on Acoustic Emission-2017* vol 218 (Springer Proceedings in Physics) pp 25–36
[22] Wei L, Jiang M S, Lü S S, Su C H, Luo Y X, Shen J S and Jia L 2020 Hypervelocity impact monitoring and location identification on aluminum plate based on FBG sensing system *Optoelectron. Lett.* **16** 306–12
[23] Van Steen C, Pahlavan L, Wevers M and Verstrynge E 2019 Localisation and characterisation of corrosion damage in reinforced concrete by means of acoustic emission and X-ray computed tomography *Constr. Build. Mater.* **197** 21–9